

## Research papers

## A knowledge-guided LSTM reservoir outflow model and its application to streamflow simulation in reservoir-regulated basins



Runting Chen<sup>a</sup>, Dagang Wang<sup>a,b,\*</sup>, Yiwen Mei<sup>a,b</sup>, Yongen Lin<sup>a</sup>, Zequn Lin<sup>a</sup>, Zhi Zhang<sup>a</sup>, Shengjie Zhuang<sup>a</sup>, Jinxin Zhu<sup>a,b</sup>, Jonghun Kam<sup>c</sup>, Yiping Wu<sup>d</sup>, Guoping Tang<sup>a,b</sup>

<sup>a</sup> School of Geography and Planning, Sun Yat-sen University, Guangzhou, China

<sup>b</sup> Carbon-Water Research Station in Karst Regions of Northern Guangdong, School of Geography and Planning, Sun Yat-sen University, Guangzhou, Guangdong, China

<sup>c</sup> Division of Environmental Science and Engineering, Pohang University of Science and Technology (POSTECH), Pohang 37673 South Korea

<sup>d</sup> School of Human Settlements & Civil Engineering, Xi'an Jiaotong University, China

## ARTICLE INFO

## Keywords:

Knowledge-guided  
LSTM  
Reservoir regulation  
Streamflow simulation  
Bootstrap  
Error propagation

## ABSTRACT

Accurate reservoir outflow simulation is crucial for modeling streamflow in reservoir-regulated basins. In this study, we introduce a knowledge-guided Long Short-Term Memory model (KG-LSTM) to simulate the outflow of reservoirs-Fengshuba, Xinfengjiang, and Baipenzhu in the Dongjiang River Basin, China. KG-LSTM is built on the standard hyperparameters-optimized-LSTM and the loss function considering reservoir operation knowledge. Model uncertainty is analyzed using the bootstrap method. We then propose a hybrid approach that combines KG-LSTM with the Three-parameter monthly hydrological Model based on the Proportionality Hypothesis (KG-LSTM-TMPH) for streamflow simulation. The propagation of inflow errors to outflow simulations is studied across the three reservoirs. Results show that KG-LSTM enhances accuracy and reduces uncertainty in outflow simulations for three reservoirs compared to LSTM, particularly for the multi-year regulated Xinfengjiang Reservoir: KG-LSTM improves Nash-Sutcliffe efficiency (NSE) from 0.59 to 0.64, reduces root mean squared error (RMSE) from 55.59 m<sup>3</sup>/s to 54.84 m<sup>3</sup>/s, and decreases the uncertainty index relative width (RW) from 0.55 to 0.51 during the testing period. For streamflow simulations at four downstream hydrological stations, the hybrid model KG-LSTM-TMPH achieves NSE values above 0.87 and outperforms LSTM-TMPH, particularly in the dry season. Inflow errors impact outflow most significantly for the Xinfengjiang Reservoir in April and May, for the Fengshuba Reservoir throughout the year, and for the Baipenzhu Reservoir in July and August. This study enhances reservoir outflow modeling by integrating reservoir operation knowledge with deep learning. The hybrid KG-LSTM-TMPH approach shows practical potential for streamflow simulation in reservoir-regulated basins, offering valuable applications for water resource management.

## 1. Introduction

As global demand for water resources continues to increase, reservoirs play a crucial role in water resources management, which significantly influence the hydrological processes and ecosystems of rivers (Hanasaki et al., 2006; Wu and Chen, 2012). The outflow of a reservoir is primarily influenced by factors such as electricity generation, irrigation, and water demand related to human activities, which in turn evidently alter the natural downstream streamflow process (Liu et al., 2019). Traditional hydrological models typically lack the module to account for the impact of reservoir, thereby limiting their applicability in simulate streamflow in reservoir-regulated basins. This underscores the necessity

of developing accurate reservoir models to improve streamflow simulation (Nohara and Hori, 2018; Turner et al., 2021; Wang et al., 2019).

Traditional reservoir models can be divided into two categories. The first category simulates reservoir outflow by formulating reservoir's functionality formulation, such as irrigation (Hanasaki et al., 2006), flood control (Zhao et al., 2016), and hydropower generation (Wu and Chen, 2012). Wu and Chen (2012) identified critical reservoir water level for hydropower generation, which determines whether to increase or decrease the outflow. They use the long-term average outflow, current storage, critical storage and other specific storage to define their model. While this approach offers clarity and convenience, it struggles to accurately capture the outflow due to complex operation rules of

\* Corresponding author.

E-mail address: [wangdag@mail.sysu.edu.cn](mailto:wangdag@mail.sysu.edu.cn) (D. Wang).

reservoirs. This limitation arises from the simplicity of formulations and the frequent unavailability of downstream water demand data typically used in modeling (Chang and Guo, 2020; Turner et al., 2021). The second category focuses on maximizing outflow benefit by identifying the global optimum among different objective functions, such as minimizing the days of water deficiency, reducing flood risk, and maximizing the hydropower generation (Haddeland et al., 2006). These objective functions are generally represented by straightforward variables; for example, the deficit of irrigation demand function are defined as the number of the day when target outflow is lower than the demand (Anand et al., 2018). This model is effective for determining optimal operation schemes under ideal historical situations but is less suitable for the real-time simulation due to high computational costs, complex actual conditions and a lack of water demand data.

Compared to traditional reservoir models, machine learning (ML) is able to efficiently learn complex operational rules by extracting information from hydrological and reservoir operation data in the absence of water demand data (Allawi et al., 2018; García-Feal et al., 2022; Qie et al., 2023; Soria-Lopez et al., 2023). Deep learning, a subtype of ML, is particularly well-suited for handling complex, multi-factor problems and is more efficient in training compared to other ML models (Ma et al., 2019; Peng et al., 2019). Among the different deep learning models, Long Short-Term Memory model (LSTM) is skilled in time series prediction, making it particularly well-suited for building reservoir models. Research has shown that LSTM outperforms other ML models in simulating reservoir outflow across different time scales and flow conditions (García-Feal et al., 2022; Ozdogan-Sarikoc et al., 2023; Zhang et al., 2018). However, these studies often overlook the analysis of model uncertainty, which can lead to risk of downstream flood and water shortage when used in reality. Combining LSTM with the bootstrap method can provide reliable uncertainty quantification for streamflow simulation (Kumar et al., 2015; Wang et al., 2022), with potential for application in reservoir outflow simulation.

As a black-box model, LSTM lacks the inherent knowledge of reservoir operation, which may result in issues like generating unrealistic values (e.g., negative flow), hindering its ability to accurately simulate reservoir outflow (Zheng et al., 2022). To overcome this limitation, Karpatne et al. (2017) introduces embedding knowledge into the loss function of LSTM model to prevent it from learning misleading patterns. Zheng et al. (2022) employed fundamental reservoir knowledge into the loss function of the LSTM model, such as the water balance, outflow boundaries, and monotonicity of reservoir outflow variation. This approach demonstrates that integrating relevant knowledge mitigates negative outflow and better captures reservoir operation compared to LSTM without guidance. However, this research did not consider other important reservoir functions, such as flood control, impoundment, and replenishment. Incorporating these functions could lead to a more comprehensive and realistic loss function for LSTM-based reservoir models, potentially enhancing physical relevance of reservoir outflow simulations.

In this study, we develop the knowledge-guided LSTM (KG-LSTM) for reservoir outflow simulation with the loss function considering knowledge of multiple reservoir functions and operation rules, while a traditional reservoir outflow model level pool scheme (LPS) is used as a benchmark model. We then use the bootstrap method to evaluate the uncertainty of KG-LSTM. Subsequently, we simulate reservoir inflow and streamflow in the sub-basins between reservoirs and downstream stations using the Three-Parameter Monthly Hydrological Model Based on the Proportionality Hypothesis (TPMH) (Zou et al., 2023), combined with the KG-LSTM outflow for streamflow simulation in reservoir-regulated basins. Finally, we analyze the propagation of inflow errors to outflow simulations through the KG-LSTM model. The remaining of this paper is structured as follows: Section 2 introduces the study area and data. Section 3 presents the methodologies for developing the KG-LSTM reservoir outflow model, establishing LPS as the benchmark model, creating the hybrid model for streamflow simulation, and

evaluating model accuracy and uncertainty. The results are presented in Section 4, and followed by discussions in Section 5. Finally, conclusions are drawn in Section 6.

## 2. Study area and data

### 2.1. The Dongjiang River basin

The Dongjiang River is a river system in the Pearl River Basin, flowing from northeast to southwest. The Xinfengjiang Reservoir (XFJR), the Fengshuba Reservoir (FSBR) and the Baipenzhu Reservoir (BPZR) are three major multi-purpose reservoirs with 11,740 km<sup>2</sup> total catchment area, accounting for 33.2 % of the Dongjiang River Basin. The total storage capacity of the three reservoirs is 17.048 billion m<sup>3</sup>, with the XFJR being the largest and serving as a multi-year regulated reservoir, while the FSBR and BPZR function as non-multi-year regulated reservoirs. The information of the three reservoirs is presented in Table 1, with a detailed analysis of their functions provided in Section 3.1.3. The basin's key hydrological stations—Longchuan, Heyuan, Lingxia, and Boluo—are situated along the river from upstream to downstream. The flow at these stations is significantly influenced by the three reservoirs, making accurate streamflow simulation essential for effective water resource planning throughout the basin. To facilitate water resource management, the year can be divided into two seasons: the flood season (April to September), which receives approximately 80% of the annual rainfall, and the dry season (October to March), which accounts for approximately 20%. According to the Hydrological Department of Dongjiang River Basin, the entire basin has been divided into seven sub-basins based on the region's terrain, as shown in Fig. 1.

### 2.2. Data

Three types of data are used in this study, including meteorological forcing data, reservoir data, and streamflow data. The meteorological forcing data, covering the period from 1961 to 2010, consists of daily precipitation records from 65 rainfall stations and 7 meteorological stations, along with potential evaporation records from the latter stations. Daily streamflow data are collected from Longchuan, Heyuan, Lingxia, Boluo hydrological stations from 1961 to 2010. The reservoir data includes daily inflow, outflow, and water level, spanning from 1961 to 2010 for the XFJR, from 1974 to 2010 for the FSBR, and from 1986 to 2010 for the BPZR, while the static characteristic information of three reservoirs is also used, namely elevation-capacity curves and flood control levels. Except for the seven meteorological stations, which are sourced from China's National-Level Surface Meteorological Stations V3.0, the other data are provided by the Hydrological Department of the

**Table 1**  
The information of the three reservoirs.

	XFJR	FSBR	BPZR
Control drainage area (km <sup>2</sup> )	5,734	5,150	856
Total storage capacity (10 <sup>6</sup> m <sup>3</sup> )	13,896	1,932	1,220
Dead storage (10 <sup>6</sup> m <sup>3</sup> )	4,307	285	190
Dead water level (m)	93	128	62
Flood control level (m)	Apr-Sep: 114-116, Oct-Mar: 116	Apr-Sep: 161-164, Oct-Mar: 163-166	Annual: 76
Regulation capability	multi-year regulated	incompletely yearly regulated	incompletely multi-year regulated
Reservoir function	Water supply, flood control and hydropower generation		

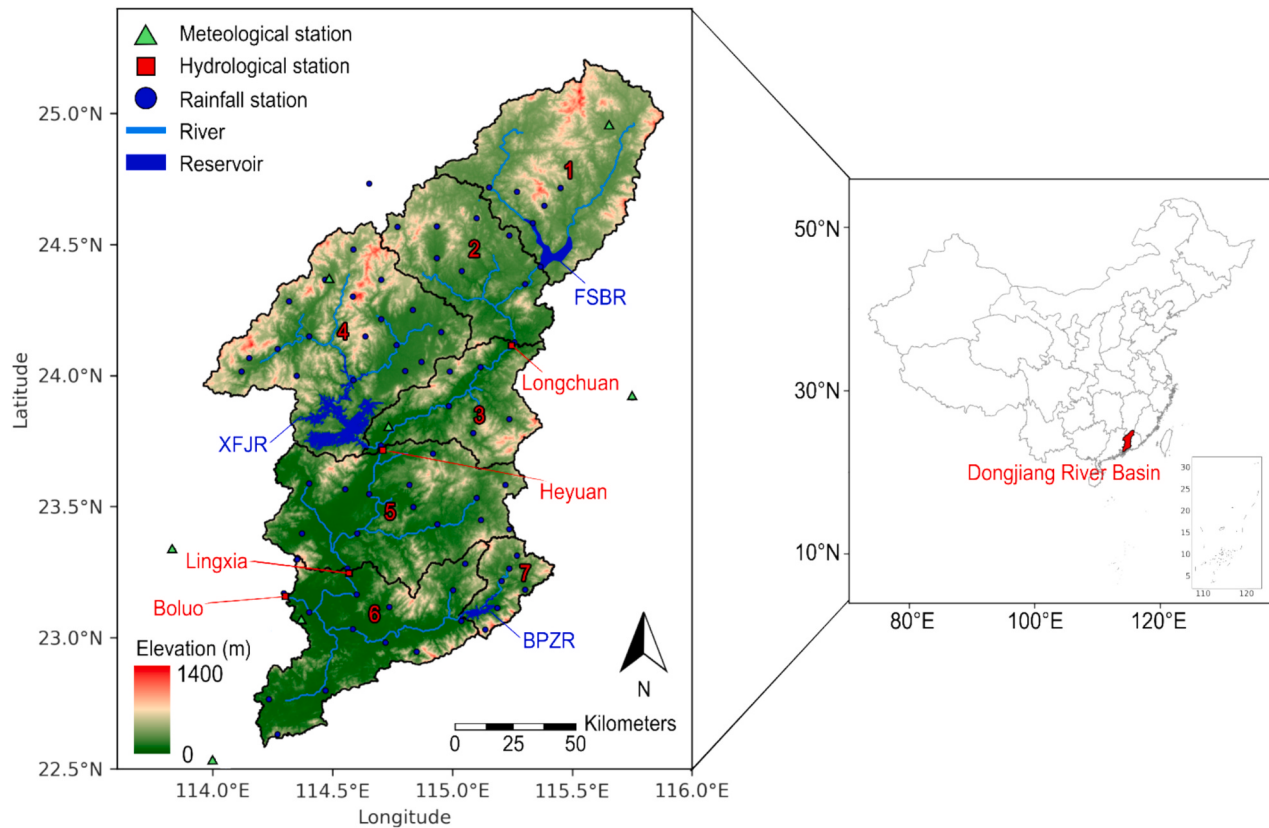


**Fig. 1.** The map of Dongjiang River Basin. Seven sub basins are divided by solid black lines.

Dongjiang River Basin. The locations of the stations are shown in Fig. 1. During data preprocessing, all daily data are aggregated to monthly scale. The precipitation and potential evapotranspiration data from the stations are then interpolated using the kriging method and the radial basis function, respectively, and then averaged across each sub-basin.

### 3. Methodology

#### 3.1. Knowledge-guided long Short-Term Memory (KG-LSTM)

As shown in Fig. 2, to construct the KG-LSTM model, we first select the input variables that impact reservoir outflow. We then use Particle Swarm Optimization to identify the optimal hyperparameters for the standard LSTM. The hyperparameters of KG-LSTM are kept the same as those of the standard LSTM to assess whether the knowledge-guided loss function can further improve model performance. The loss term (mean squared error of reservoir outflow simulation) for LSTM are combined with the knowledge-guided loss terms, which considers reservoir function and operation rules, to build the loss function for KG-LSTM. We divide data into 75 % for training and 25 % testing LSTM and KG-LSTM. The data time spans for the XFJR, FSBR, BPZR are from January 1961 to December 2006, from January 1974 to December 2006, from January 1986 to December 2006, respectively.

##### 3.1.1. Model inputs

For non-multi-year regulation reservoirs, the input variables for the standard LSTM include: (1) Reservoir inflow ( $Q_i$ ), representing the hydrological processes in the upstream basin, is crucial for outflow determination since it is directly influencing the change in reservoir storage and water level (Yang et al., 2019); (2) Reservoir water level ( $W_l$ ), where water level states are essential for reservoir operation decisions. For example, reservoir outflow will be increased to mitigate flood risk when the water level is high during the flood season (Zheng

et al., 2022); (3) Month ( $Mo$ ) is selected, since the reservoir function differs monthly. For example, the flood control function is prioritized during the flood season while the replenishment function is mainly considered during the dry season (Zhang et al., 2018).

For multi-year regulated reservoirs, additional input variables are added to better reflect the complex rules governing reservoir outflow: (1) Reservoir outflow ( $Q_o$ ) can be used to extract the information of recent reservoir operation for LSTM model learning (Zhang et al., 2018; Zheng et al., 2022); (2) Downstream station flow ( $Q_d$ ) can indirectly reflect water demand in downstream. For example, when downstream flow is low, the reservoir increases outflow to meet downstream water demand (Wu and Chen, 2012); (3) Hydrological year ( $Yr$ ) is selected, since the reservoir will adjust outflow based on the water amounts to regulate multi-year water resource (Wu and Chen, 2012). The classification of wet, normal, dry year is determined by reservoir inflow percentiles that are greater than the 80th percentile, between the 20th and 80th percentiles, and below the 20th percentile, respectively, and represented as -1, 0, and 1 as input variables.

The model's output is the reservoir outflow for the current month ( $Q_{ot}$ ). The time lag of input variables is determined based on the Pearson correlation coefficient with  $Q_{ot}$  (Sushanth et al., 2023). We used an absolute Pearson correlation coefficient of 0.3 as the threshold to determine the time lags. As reservoir outflow is a multifactorial and nonlinear decision process, we chose this threshold to capture a potential correlation between the influencing variables and the outflow. Additionally, we aimed to include more variables to enhance information available for LSTM learning. The input variables for the three reservoirs are as follows: The inflow of the previous and current months ( $Q_{it-1}, Q_{it}$ ), the water level of the previous month ( $Wl_{t-1}$ ), and the current month ( $Mo$ ). For the XFJR, a multi-year regulated reservoir, additional input variables include the outflow of the previous two months and the previous month ( $Q_{ot-2}, Q_{ot-1}$ ), the water level of the previous two months ( $Wl_{t-2}$ ), the downstream flow of the previous month ( $Qd_{t-1}$ ), and the

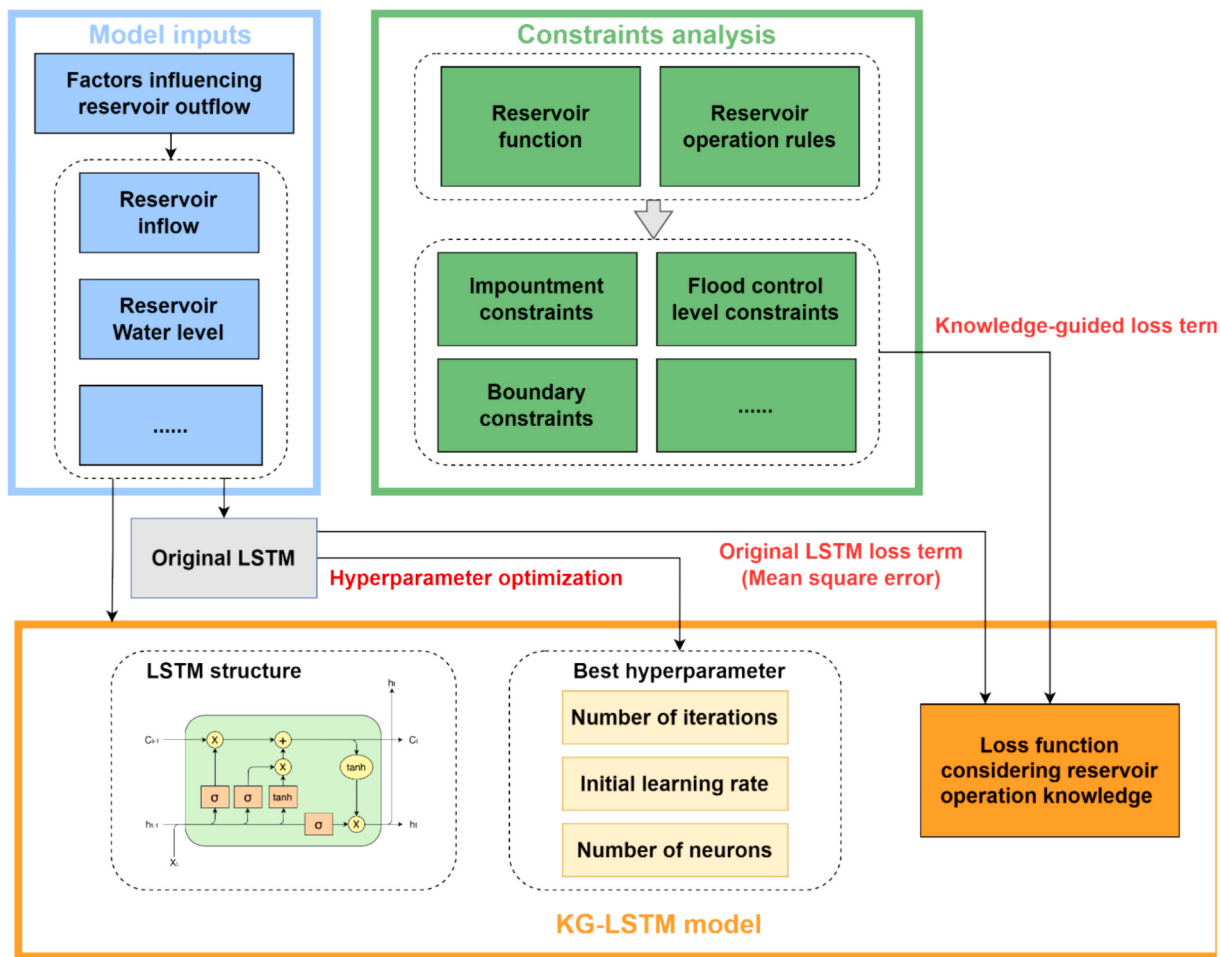


**Fig. 2.** Construction of KG-LSTM, including model inputs, hyperparameter optimization for the standard LSTM, constraints analysis, and establishment of the loss function considering reservoir operation knowledge.

hydrological year (Yr). The storage and water level for the current month are calculated by the water balance equations (Eqs. 1 and 2) and elevation-capacity curves,

$$\Delta V_t = (Q_{i_t} - Q_{o_t}) * \Delta t \quad (1)$$

$$V_t = V_{t-1} + \Delta V_t \quad (2)$$

where  $\Delta t$  is the total seconds of the month;  $\Delta V_t$  is the change in reservoir volume for the month;  $V_t$  and  $V_{t-1}$  represent the reservoir volume for the current month and the previous month, respectively.

### 3.1.2. Construction of the standard LSTM

The Long Short-Term Memory (LSTM) network is an improved version of the Recurrent Neural Network. It addresses the vanishing gradient problem during model training by introducing additional forget gates (Hochreiter and Schmidhuber, 1997). This enhanced LSTM network is capable of learning long-term dependencies in time series data. The structure of the LSTM model includes forget, input, and output gates, along with memory cells. The forget gate disregards irrelevant past information from the cell during training. The input gate updates the cell state values with new values at the current time step. The output gate controls the cell state values passed through the hidden layer. Memory cells are responsible for storing long-term memory information. Mean squared error is used as the loss function of the standard LSTM. A detailed description of the LSTM computation process can be found in Xu et al. (2021).

To determine the optimal performance of the standard LSTM, we use

Particle Swarm Optimization (PSO) to optimize the number of neurons, learning rate, and number of iterations in the standard LSTM. PSO has the advantages of minimal requirements on the objective function and fast convergence speed, making it well-suited for LSTM hyperparameter optimization (Xie et al., 2019; Xu et al., 2022). The ranges for these hyperparameters are set as follows: number of neurons [128, 256], number of iterations [100, 200], and initial learning rate [0.001, 0.01]. The optimized values for the XFJR are 293 neurons, 155 iterations, and initial learning rate of 0.0007. For the FSBR, the optimized values are 79 neurons, 263 iterations, and initial learning rate of 0.0015. For the BPZR, the optimized values are 28 neurons, 197 iterations, and initial learning rate of 0.0015. Other hyperparameters, such as the use of one hidden layer, ADAM optimizer, and a batch size of 4, remain consistent across all models.

### 3.1.3. Loss function considering reservoir operation knowledge

To establish knowledge-guided loss function, we first analyze the reservoir's function and operation rule. We then define constraints related to dead water level, flood control level, impoundment and replenishment, and boundaries limits.

**The dead water level constraints:** Storage below the dead water level is referred to as dead storage, which is primarily used for sediment accumulation and to increase the water head. Dead storage is usually avoided in normal operations. As shown in Fig. 3, the water levels of the FSBR and BPZR typically remain above the dead water level, whereas this is not always the case for the XFJR. This is because the dead storage capacity of the XFJR (43.07 billion m<sup>3</sup>) is much larger than that of the

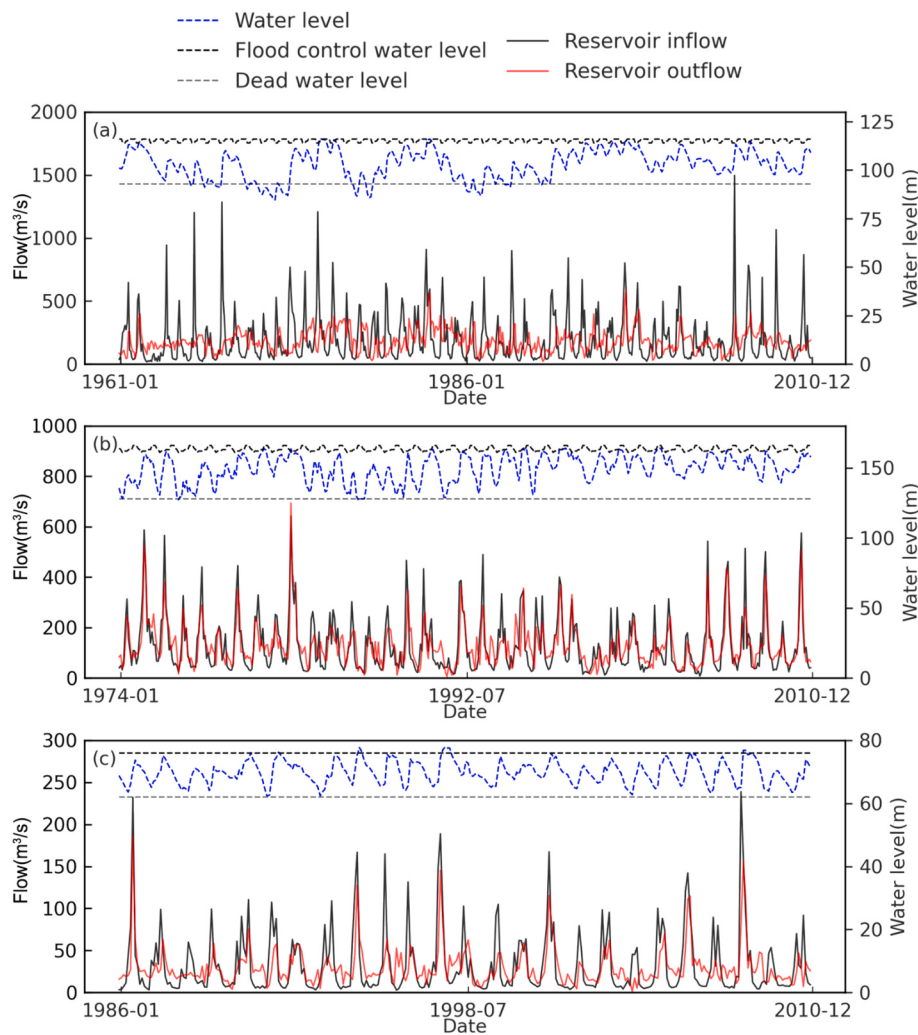


**Fig. 3.** The inflow, outflow, and water level for (a) XFJR, (b) FSBR, and (c) BPZR from completion to 2010.

FSBR (285 million m<sup>3</sup>) and BPZR (190 million m<sup>3</sup>). Consequently, the dead storage of the XFJR is frequently utilized during drought conditions. Therefore, dead water level constraints are only applied to the FSBR and BPZR, as formulated below,

$$Wl_t \geq Wl_{\text{dead}} \quad (3)$$

where  $Wl_{\text{dead}}$  represents the dead water level.

The flood control level constraints: To ensure that the reservoir can accommodate potential floods, the flood control level is the highest water level allowed for impoundment. As shown in Fig. 3, the three reservoirs have not exceeded the flood control water level for most of the time. The formulation of the flood control level constraints is as follows,

$$Wl_t \leq Wl_{t,\text{flood}} \quad (4)$$

**Table 2**

The multi-year average hydrological data for the dry season (October to March) and flood season excluding April and May (June to September) for dry years (inflow below 20th percentile) and non-dry years (above the 20th percentile).

		XFJR Non-dry year	Dry year	FSBR Non-dry year	Dry year	BPZR Non-dry year	Dry year
October to March	Downstream streamflow without reservoir (m <sup>3</sup> /s)	271.56	162.03	126.73	85.48	39.97	16.68
	Outflow (m <sup>3</sup> /s)	195.08	145.54	97.19	63.01	24.04	8.55
	Inflow (m <sup>3</sup> /s)	93.88	56.51	73.91	45.21	10.89	8.13
June to September	Replenishment ratio	0.37	0.55	0.18	0.21	0.33	0.03
	Inflow (m <sup>3</sup> /s)	335.77	167.91	201.59	107.67	77.64	42.19
	Outflow (m <sup>3</sup> /s)	216.93	137.28	182.36	96.58	55.28	22.25
	Storage ratio	0.35	0.18	0.10	0.10	0.29	0.47

Data in this table include downstream streamflow without reservoir, reservoir inflow and outflow, replenishment ratio and storage ratio. The downstream flow without reservoir of reservoirs-FSB, XFJ and BPZ in the table refer to sub-basin 2, 3, 6 in Fig. 1., respectively. Downstream streamflow without reservoir = Downstream streamflow – upstream reservoir outflow + upstream reservoir inflow, Replenishment ratio = (reservoir outflow – reservoir inflow) / downstream streamflow without reservoir, Storage ratio = (reservoir inflow – reservoir outflow) / reservoir inflow.

where  $Wl_{t,flood}$  represents the flood control water level for the current month.

The impoundment and replenishment constraints: During the flood season, reservoir operators will reduce outflow to impound water while maintaining flood control functionality, and increase outflow to supply water downstream in the dry season. To further analyze these functions, the multi-year average values of reservoir inflow, outflow, and downstream flow for different periods and hydrological years are summarized in Table 2, indicating the following: (1) From October to March, the multi-year average outflow from the three reservoirs exceeds the inflow, indicating that the reservoirs are releasing water downstream to meet the demand. This aligns with their primary function of supplying water during the dry season in the Dongjiang River Basin. During this period, the replenishment ratio for the BPZR clearly varies between dry and non-dry years, suggesting the need for a smaller coefficient for the replenishment loss term in its loss function to avoid unreasonable penalties. (2) From June to September, the multi-year average inflow to the three reservoirs exceeds the outflow, indicating effective water impoundment. The FSBR has the lowest impoundment ratio among the three reservoirs, warranting a reduction in its coefficient for the impoundment loss term. (3) The XFJR demonstrates capabilities for multi-year regulation. Compared to non-dry years, in dry years, it provides more water resources to downstream areas by reducing impoundment (with the storage ratio decreasing from June to September) and increasing replenishment (with the replenishment proportion rising from October to March). Therefore, adjustments should be made to the coefficients of the impoundment and replenishment loss terms for the XFJR based on the hydrological years. In contrast, such adjustments are not necessary for the BPZR and FSBR due to their relatively smaller storage and regulation capacities. The formulations for the impoundment and replenishment constraints are as follows,

$$Qi_t \leq Qo_t, t \in [6, 7, 8, 9] \quad (5)$$

$$Qi_t \geq Qo_t, t \in [1, 2, 3, 10, 11, 12] \quad (6)$$

Additionally, the replenishment and impoundment constraints are not considered in April and May, as this period marks the onset of the flood season, with high uncertainty in basin streamflow. Reservoir operators will adjust their operational strategy flexibly: they will continue replenishing if the basin faces water scarcity, or switch to impoundment when the reservoir water level is low and the basin streamflow is sufficient to meet water demand.

The boundaries constraints: For ecological protection, there is a minimum outflow that reservoir must ensure, while the maximum outflow is regulated for protecting downstream from flood. Therefore, the reservoir outflow should have upper and lower bounds, with formulations as,

$$Qo_l \leq Qo_t \leq Qo_u \quad (7)$$

**Table 3**

The coefficients of different loss terms settings for the three reservoirs.

Loss term coefficient	XFJR	FSBR	BPZR			
	KG-LSTM	LSTM	KG-LSTM	LSTM	KG-LSTM	LSTM
$\lambda_{LSTM}$	1	1	1	1	1	1
$\lambda_{flood}$	10,000		10,000	\	10,000	\
$\lambda_{imp}$	0.1&0.05		0.01	\	0.1	\
$\lambda_{rep}$	0.1&0.15		0.1		0.05	
$\lambda_{boundary}$	1	\	1	\	1	\
$\lambda_{dead-level}$	\	\	10,000		10,000	\

$\lambda_{imp}$  and  $\lambda_{rep}$  are adjusted in the XFJR to embody the multi-year regulated function, left for non-dry and right for dry hydrological years.

where  $Qo_l$  and  $Qo_u$  respectively denote the lower and upper bounds of the reservoir outflow, respectively.

Based on the constraint analysis mentioned above, we establish a KG-LSTM loss function as follows:

$$\begin{aligned} loss_{KG-LSTM} &= \lambda_{LSTM} loss_{LSTM} + \lambda_{flood} loss_{flood} + \lambda_{imp} loss_{imp} + \lambda_{rep} loss_{rep} \\ &\quad + \lambda_{boundary} loss_{boundary} + \lambda_{dead-level} loss_{dead-level} \\ loss_{LSTM} &= \frac{1}{n_t} \sum_{t=1}^{n_t} (\widehat{Qo}_t - Qo_t)^2 \\ loss_{flood} &= \frac{1}{n_t} \sum_{t=1}^{n_t} (\widehat{Wl}_t - Wl_{t,flood})^2 \text{ if } t \in [6, 7, 8, 9], \widehat{Wl}_t > Wl_{t,flood} \\ loss_{imp\&rep} &= \frac{1}{n_t} \sum_{t=1}^{n_t} (\widehat{Qo}_t - Qi_t)^2 \text{ if } \begin{cases} t \in [6, 7, 8, 9], \widehat{Qo}_t > Qi_t \\ t \in [1, 2, 3, 10, 11, 12], \widehat{Qo}_t < Qi_t \end{cases} \\ loss_{dead-level} &= \frac{1}{n_t} \sum_{t=1}^{n_t} (\widehat{V}_t - V_{dead})^2 \text{ if } \widehat{Wl}_t < Wl_d \\ loss_{boundary} &= \frac{1}{n_t} \sum_{t=1}^{n_t} g(\widehat{Qo}_t) \\ g(\widehat{Qo}_t) &= \begin{cases} (\widehat{Qo}_t - Qo_u)^2 \text{ if } \widehat{Qo}_t > Qo_u \\ 0 \text{ if } Qo_l < \widehat{Qo}_t < Qo_u \\ (\widehat{Qo}_t - Qo_l)^2 \text{ if } \widehat{Qo}_t < Qo_l \end{cases} \end{aligned} \quad (8)$$

where  $loss_{KG-LSTM}$  is the loss function of KG-LSTM,  $loss_{LSTM}$  is the mean squared error between the simulated and observed outflow,  $loss_{flood}$  is the penalty if the reservoir water level exceeds the flood control level,  $loss_{imp\&rep}$  is the penalty if reservoir fails to impound water during the flood season or replenish during the dry season,  $loss_{boundary}$  is the penalty for failing to meet the outflow boundary constrain,  $loss_{dead-level}$  is the penalty if reservoir water level drop below the dead level, and  $\lambda$  is the coefficient for these loss terms,  $n_t$  is the length of the simulation time,  $Qo_t$  and  $\widehat{Qo}_t$  represent the observed and simulated outflows at time  $t$ , respectively,  $Wl_t$  and  $\widehat{V}_t$  represent the simulated water level and storage, respectively. Note that the coefficient  $\lambda$  for those loss terms were determined through trial and error as well as reservoir functionality analysis (Zheng et al., 2022). The final values of these coefficients are listed in Table 3.

### 3.2. Benchmark model

To show the advantages of LSTM and KG-LSTM in reservoir outflow simulation compared to the traditional reservoir model, Level Pool scheme (LPS) is used as a benchmark model. This model simplifies the outflow process by disregarding the internal complexity, and focusing solely on the water balance between inflow and outflow. LPS tracks water level changes over time, with outflow separated into weir overflow  $Qo_{w,t}$  and gate-controlled flow  $Qo_{o,t}$  (Eq. 9). Weir overflow only happens when the reservoir water level  $Wl$  is higher than weir height  $Wl_{max}$  (Eq. 10), while gate-controlled flow can happen anytime (Eq. 11). Water levels are calculated using level-capacity curve fitting by history data. More detailed information about the LPS method can be found in Goodell and Wahlin (2009). The outflow of LPS is calculated as follows:

$$Qo_t = Qo_{w,t} + Qo_{o,t} \quad (9)$$

$$Qo_{w,t} = \begin{cases} Cw \times WL \times WL^{\frac{3}{2}} \text{ if } WL > WL_{max} \\ 0 \text{ if } WL < WL_{max} \end{cases} \quad (10)$$

$$Qo_{o,t} = Co \times Oa \times \sqrt{2gh} \quad (11)$$

where  $Q_{o,w,t}$  is weir overflow,  $Q_{o,g,t}$  is gate-controlled flow,  $WL$  is the length of the weir (m),  $WL_{max}$  is the maximum height before the weir begins to spill (m),  $C_w$  is the weir coefficient,  $C_o$  is the orifice coefficient,  $Oa$  is the orifice area ( $m^2$ ), and  $g$  is the acceleration due to gravity ( $m/s^2$ ).

### 3.3. Hybrid approach

To simulate streamflow at stations, we use a hybrid approach that combines reservoir models with a hydrological model. The process is as follows: First, the hydrological model simulates reservoir inflow and streamflow in the sub-basins between reservoirs and downstream stations using meteorological forcing data. Next, the simulated reservoir inflow, along with other inputs, is fed into the reservoir model to generate reservoir outflow. Finally, we combine the reservoir outflow with sub-basins streamflow between the reservoirs and downstream stations to produce streamflow at those downstream stations.

For the hydrological model, TMPH is a lumped, monthly-scale hydrological model based on water-energy coupled balance equations, proportional assumptions and with three parameters: the initial water loss ratio, water loss capacity of the basin, and evapotranspiration parameter. TMPH calculates the basin streamflow considering processes such as rainfall, evaporation, and groundwater flow, showing good predictive results in the Han River Basin (Zou et al., 2023). The inputs of TMPH include rainfall data, evaporation data, and characteristic parameters of hydrological units including the area and initial water storage in soil. We divide data into 75 % for model calibration and 25 % for validation. Details on model simulations across 7 sub-basins can be found in Section 4.2.1. In this study, we select calibrated TMPH as the hydrological model for seven sub-basins and integrate them with the trained reservoir models to construct hybrid models, including KG-LSTM-TMPH, LSTM-TMPH, and LPS-TMPH.

### 3.4. Model evaluation

We use root mean squared errors (RMSE), Pearson's correlation coefficients (r) and the Nash-Sutcliffe efficiency (NSE) (Nash and Sutcliffe, 1970) to evaluate the accuracy of the reservoir, hydrological, and hybrid models. Additionally, we use water balance index (WBI) (Zheng et al., 2022) to assess the physical consistency of the reservoir models. The r and NSE values closer to 1 indicate better simulation, while a WBI closer to 0 reflects better alignment with the actual reservoir water balance. RMSE with smaller values indicates higher accuracy. The metrics are computed as follows:

$$NSE = 1 - \frac{\sum_{t=1}^{n_t} (\widehat{Q}_t - Q_t)^2}{\sum_{t=1}^{n_t} (Q_t - \bar{Q}_t)^2} \quad (11)$$

$$RMSE = \sqrt{\frac{1}{n_t} \sum_{t=1}^{n_t} (\widehat{Q}_t - Q_t)^2} \quad (12)$$

$$r = \sum_{t=1}^{n_t} (\widehat{Q}_t - \bar{\widehat{Q}}_t) \frac{(\widehat{Q}_t - \bar{Q}_t)}{\sqrt{\sum_{t=1}^{n_t} (\widehat{Q}_t - \bar{\widehat{Q}}_t)^2 \sum_{t=1}^{n_t} (Q_t - \bar{Q}_t)^2}} \quad (13)$$

$$WBI = \left| 1 - \frac{\sum_{t=1}^{n_t} \widehat{Q}_t}{\sum_{t=1}^{n_t} Q_t} \right| \quad (14)$$

where  $n_t$  represents the length of the simulation period;  $Q_t$  and  $\widehat{Q}_t$  denote the observed and simulated outflows at time t, respectively.

The uncertainty of reservoir outflow can lead to risks as downstream flood and water shortage. To evaluate the uncertainty of the KG-LSTM and LSTM reservoir models, we use the bootstrap method. Bootstrap is a statistical resampling technique used to assess the stability and sam-

pling distribution of a statistic by generating virtual datasets from the standard data, without requiring assumptions about the underlying distribution (Zhang et al., 2014). Bootstrap is well-suited for moderately sized independent samples when statistical information is limited (Gopala et al., 2019) and can provide reliable uncertainty quantification of streamflow prediction when combined with LSTM (Wang et al., 2022). In this study, the uncertainty interval is constructed using the 90 % quantiles of residuals, providing narrow and appropriate range. We resample the training dataset 100 times to train 100 models and assess their uncertainty intervals during both the training and testing phases. Coverage rate (CR), relative width (RW), relative deviation (RD) are used for uncertainty measurement (Bock et al., 2018). CR ranges from 0 to 1, with a higher CR indicating better coverage of the interval. RW measures the average ratio of uncertainty width to the predicted value. RD measures the deviation of the predicted interval's centerline from the observed flow curve. Lower values of RW and RD, closer to 0, indicates greater model stability. Their equations are as follows:

$$CR = \frac{n}{n_t} \quad (15)$$

$$RB = \frac{1}{n_t} * \sum_{t=1}^{n_t} \frac{(\widehat{Q}_{o,t}^u - \widehat{Q}_{o,t}^l)}{\widehat{Q}_{o,t}} \quad (16)$$

$$RD = \frac{1}{n_t} * \sum_{t=1}^{n_t} \left( \left| \frac{1}{2} (\widehat{Q}_{o,t}^u + \widehat{Q}_{o,t}^l) - Q_{o,t} \right| \right) / \widehat{Q}_{o,t} \quad (17)$$

where  $n$  is the number of observed values within the uncertainty interval, while  $n_t$  represents the total number of observed values.  $\widehat{Q}_{o,t}^u$  and  $\widehat{Q}_{o,t}^l$  represent the 0.05 and 0.95 quantiles of the each  $\widehat{Q}_{o,t}$  which defines the interval at time t.

## 4. Results

### 4.1. Assessment of reservoir models in simulating reservoir outflow

To compare the simulation performance of LSTM, KG-LSTM, and LPS models in simulating outflow from the three reservoirs, we summarize their accuracy in Table 4. KG-LSTM consistently demonstrates higher accuracy in both the training and testing periods. During the testing period, KG-LSTM achieves an NSE of 0.64 for the XFJR (0.05 higher than LSTM, 0.24 higher than LPS), 0.80 for the FSBR (0.02 higher than LSTM, 0.10 higher than LPS), and 0.85 for the BPZR (0.02 higher than LSTM, 0.14 higher than LPS). We observe that KG-LSTM shows the most significant improvement for the XFJR, increasing NSE from 0.59 and 0.37 to 0.64, reducing RMSE from 55.59 m<sup>3</sup>/s and 70.9 m<sup>3</sup>/s to 54.84 m<sup>3</sup>/s, and decreasing WBI from 0.05 and 0.03 to 0.00 compared with LSTM and LPS.

To further investigate the improvements made by KG-LSTM, we present the monthly time series and the kernel density curves of simulations for the three reservoirs by the three models during the testing periods in Fig. 4. For the XFJR, LPS barely capture the general patterns of reservoir outflow and often shows simulated increases and decreases that contradict observed data. This highlights the limitations of traditional models in capturing complex multi-year reservoir operation. In contrast, both KG-LSTM and LSTM more accurately capture outflow dynamics, with KG-LSTM performing better in capturing high outflow compared to LSTM (Fig. 4a). The probability density function of KG-LSTM's outflow simulation distribution shows an improvement in the frequency overestimation range from 120 to 420 m<sup>3</sup>/s existing in LSTM (Fig. 4b). This improvement is also supported by the WBI metrics, as KG-LSTM achieves a perfect score of 0.00, outperforming LSTM's score of 0.03. For the FSBR, the outflow time series simulated by KG-LSTM and LSTM aligns more closely with observed values, with KG-LSTM demonstrating superior performance (Fig. 4c). However, KG-LSTM and

**Table 4**

The performance of KG-LSTM, LSTM, and LPS in simulating outflow for the three reservoirs.

	Performance metrics	XFJR			FSBR			BPZR		
		KG-LSTM	LSTM	LPS	KG-LSTM	LSTM	LPS	KG-LSTM	LSTM	LPS
Training period	r	0.82	0.81	0.51	0.90	0.89	0.84	0.93	0.92	0.83
	RMSE( $m^3/s$ )	49.61	55.28	74.71	39.52	40.48	47.05	8.42	9.71	13.01
	NSE	0.66	0.58	0.23	0.79	0.78	0.70	0.87	0.82	0.68
	WBI	0.04	0.10	0.06	0.06	0.03	0.05	0.01	0.03	0.06
Testing period	r	0.80	0.79	0.65	0.92	0.92	0.84	0.93	0.92	0.85
	RMSE( $m^3/s$ )	54.84	55.59	70.90	35.16	36.91	42.69	8.05	8.62	11.29
	NSE	0.64	0.59	0.40	0.80	0.78	0.70	0.85	0.83	0.71
	WBI	0.00	0.05	0.03	0.12	0.14	0.01	0.01	0.00	0.11

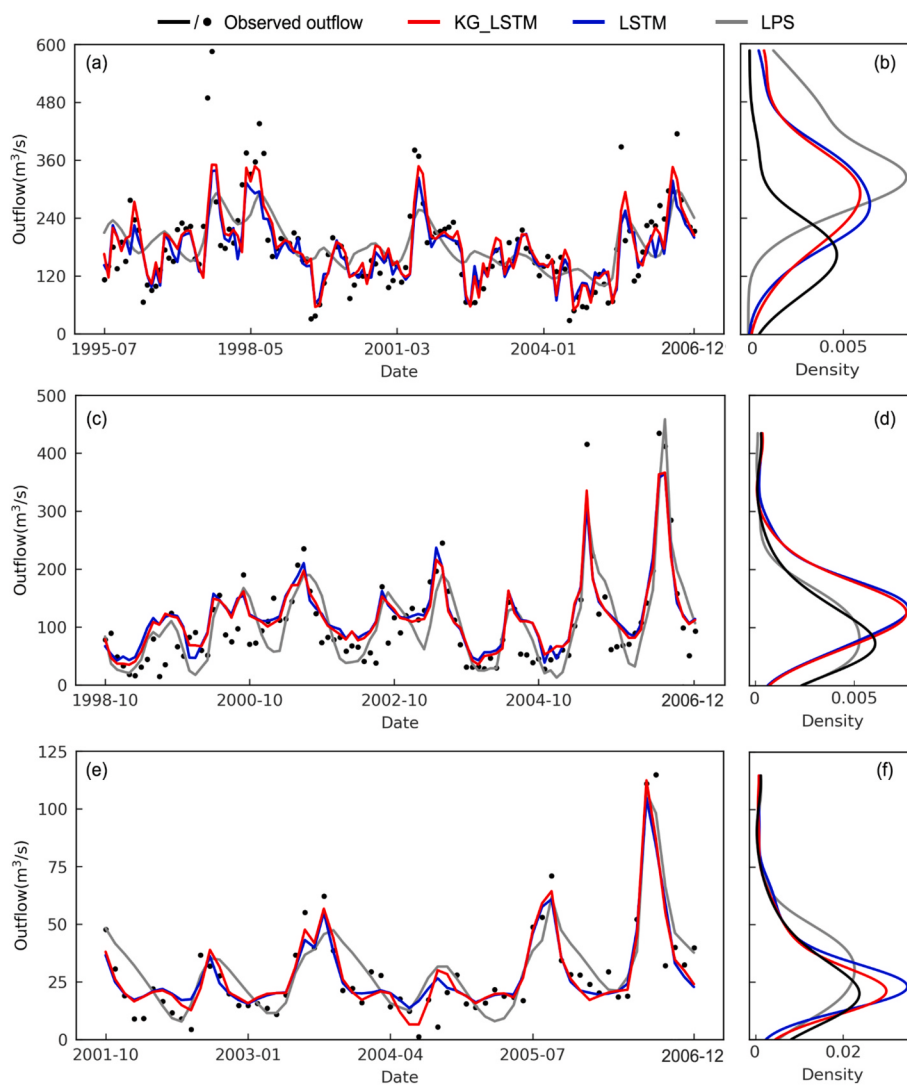


**Fig. 4.** The monthly time series and the kernel density curves of outflow simulations for XFJR (a, b), FSBR (c, d), and BPZR (e, f) by the three models.

LSTM tend to overestimate outflows higher than  $100 m^3/s$  and underestimate those below  $100 m^3/s$  compared to LPS (Fig. 4d). For the BPZR, KG-LSTM and LSTM outperform LPS in capturing both high and low flow values (Fig. 4e). Moreover, the density curves of KG-LSTM and LSTM align more closely with the observed peak, with KG-LSTM reducing the overestimation in low outflow situations compared to LSTM (Fig. 4f).

To evaluate the improvement of KG-LSTM compared to LSTM in simulation uncertainty, Fig. 5 shows 90 % confidence intervals and uncertainty metrics (CR, RW and RD) of monthly outflow for the three reservoirs during the testing period. In the XFJR (Fig. 5a, b), both KG-LSTM and LSTM achieve a CR higher than 0.60, indicating that their

uncertainty intervals cover at least 60 % of the observed values. Compared to LSTM, KG-LSTM reduces the RW by 0.04 in the testing period, producing more stable outflow simulations. In the FSBR (Fig. 5c, d), though KG-LSTM shows limited improvement compared to LSTM, both of their uncertainty intervals and median values of outflow simulation closely align with the observed outflow. This alignment confirms their reliability in capturing reservoir operation rules. Although the CR is lower than 0.50, the small RW and RD values suggest consistent performance in both models. In the BPZR (Fig. 5e, f), KG-LSTM shows a more significant improvement in RW, with reductions of 0.04 during the testing periods while maintaining the same CR. This indicates that KG-

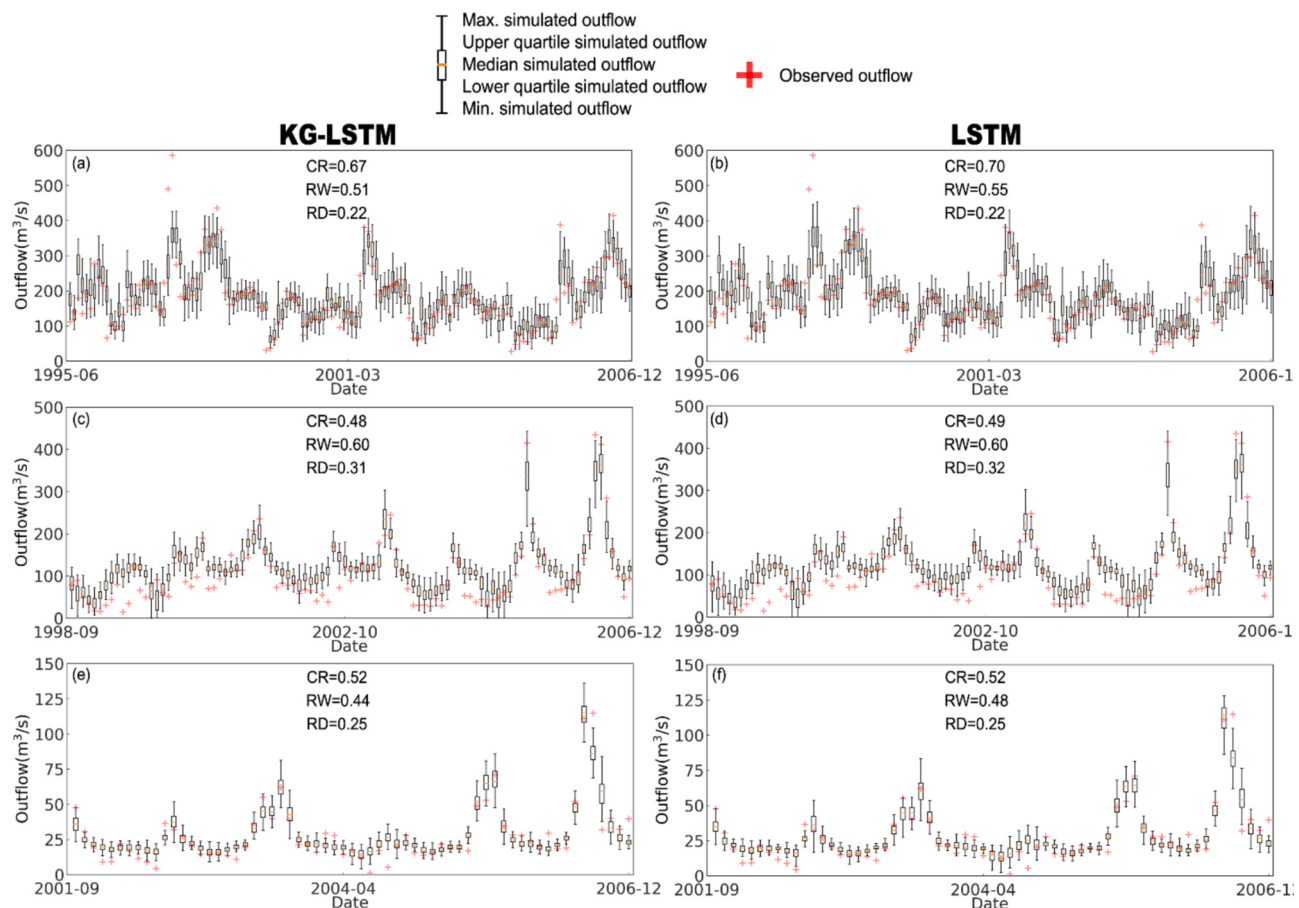


**Fig. 5.** 90% confidence intervals of outflow simulated by KG-LSTM and LSTM compared with observations during the testing periods for XFJR (a, b), FSBR (c, d) and BPZR (e, f).

LSTM based simulations are closer to observations, resulting in more stable overall model performance. As in the FSBR, despite a low CR, the model effectively captures the reservoir's outflow dynamics.

#### 4.2. Assessment of hybrid method in simulating streamflow

The streamflow at stations downstream of the reservoir is simulated by integrating the reservoir model described above with TMPH. The reservoir model simulates the outflow, while TMPH is used to simulate both the inflow into the reservoir and the streamflow for the sub-basin between the reservoir and the downstream station.

##### 4.2.1. TMPH

TMPH is assessed from two perspectives. First, the model simulated reservoir inflow is compared with observed inflow. Second, the simulated streamflow for the sub-basin between the reservoir and the downstream station, along with observed reservoir outflow, are compared with streamflow observations at downstream stations. The time spans and performance metrics during calibration and validation periods are summarized in Table 5. Taking the XFJR as an example, the TMPH inflow simulation during the validation period achieves  $r$  of 0.97, NSE of 0.94, and RMSE of  $49.44 \text{ m}^3/\text{s}$ , demonstrating strong simulation accuracy. Overall, for various regions in the Dongjiang River Basin, TMPH demonstrates good simulation performance during the validation period, with NSE exceeding 0.9 and  $r$  greater than 0.96. These results suggest that TMPH is suitable for monthly-scale streamflow simulation.

##### 4.2.2. Hybrid method

In this study, the observed meteorological data and reservoir

operation data from January 2007 to December 2010 are used as the input for three hybrid models, KG-LSTM-TMPH, LSTM-TMPH, and LPS-TMPH, to simulate streamflow at the four hydrological stations with a one-month lead time. In this period, KG-LSTM-TMPH in the outflow simulation for the XFJR, FSBR, and BPZR yields NSE values 0.70, 0.78, and 0.82, respectively, which are higher than LSTM-TMPH's values of 0.62, 0.78, and 0.78, and LPS-TMPH's values of 0.05, 0.65, and 0.75. TMPH also perform well in this period, with the NSE values 0.98, 0.96, 0.96 for the inflow simulation of the XFJR, FSBR, BPZR. Monthly streamflow time series and scatter plots for flood and dry seasons simulated by the hybrid models at four stations are shown in Fig. 6, indicating that KG-LSTM-TMPH performs best in simulating streamflow with NSE values of 0.87, 0.88, 0.91, and 0.92 for Longchuan, Heyuan, Lingxia, and Boluo stations, respectively. The most significant improvement occurs at Heyuan station (Fig. 6d), where compared to LSTM-TMPH and LPS-TMPH, NSE is increased by + 0.02 and + 0.23, RMSE is reduced  $-3.90 \text{ m}^3/\text{s}$  and  $-51.57 \text{ m}^3/\text{s}$ , respectively. During the flood season (Fig. 6b, e, h, k), the performance of KG-LSTM-TMPH is comparable to LSTM-TMPH, with both models reasonably predicting the streamflow at the stations ( $R^2 > 0.82$ ) and significantly outperforming LPS-TMPH. However, during the dry season (Fig. 6c, f, i, l), KG-LSTM-TMPH demonstrates substantial improvement over the other models, particularly at Heyuan station (Fig. 6f), where it improves the  $R^2$  by + 0.11, + 0.42 and reduces the RMSE by  $-4.22 \text{ m}^3/\text{s}$ ,  $-42.82 \text{ m}^3/\text{s}$  compared to LSTM-TMPH, LPS-TMPH, respectively. In the dry season, KG-LSTM-TMPH can efficiently reduce the underestimation in outflow compared to LSTM-TMPH across all stations.

**Table 5**

TMPH performance in simulating reservoirs inflow and streamflow across sub-basins and stations.

	Performance metrics	FSBR	XFJR	BPZR	Longchuan	Heyuan	Lingxia	Boluo
Calibration period	r	0.96	0.97	0.97	0.98	0.93	0.95	0.99
	RMSE( $m^3/s$ )	32.24	45.23	8.58	25.92	96.2	113	68.35
	NSE	0.92	0.94	0.95	0.97	0.86	0.9	0.98
Validation period	r	0.96	0.97	0.99	0.98	0.99	0.98	0.99
	RMSE( $m^3/s$ )	30.59	49.44	7.49	25.19	36.25	78.53	67.31
	NSE	0.91	0.94	0.95	0.97	0.98	0.96	0.99
Time spans	Start date	1974-01	1961-01	1986-01	1974-01	1961-01	1961-01	1986-01
	End date	2006-12	2006-12	2006-12	2006-12	2006-12	2006-12	2006-12

The inflow to FSB, XFJR, and BPZR is actually the streamflow over the sub-basins 1, 4, and 7, respectively. Longchuan: sum of sub-basin 2 streamflow and FSBR outflow. Heyuan: sum of sub-basin 3 streamflow, Longchuan streamflow and XFJR outflow. Lingxia: sum of sub-basin 5 streamflow and Heyuan streamflow. Boluo: sum of sub-basin 6 streamflow, Lingxia streamflow, and BPZR outflow. The observed reservoir outflow is used for this analysis. The sub basins locations are shown in Fig. 1.

## 5. Discussions

### 5.1. The enhanced effect by integrating reservoir operation knowledge in LSTM

In this study, we demonstrate that the KG-LSTM improves accuracy of simulated reservoir outflow and reduces uncertainty of simulations compared to the standard LSTM. The results also indicate that incorporating deep learning with a physics-based model effectively capture streamflow dynamics in reservoir-regulated basins. Our findings are consistent with the perspective presented by (Karpatne et al., 2017), who argue that the combination of theoretical knowledge with machine learning models result in more generalizable solutions. Furthermore, our results support the assertion by Shen et al. (2018) that integrating process-based models with deep learning can leverage their strengths to address hydrological challenges. While incorporating the latest reservoir operation data would be beneficial, we faced a lack of observational data after 2010, which prevented us from training and testing the reservoir models and TMPH hydrological model. When observational data after 2010 is available, it will be possible to develop an updated KG-LSTM reservoir outflow model that recognizing the change of hydrological condition and reservoir operation rules for better guiding future reservoir management and runoff simulations.

For data-driven models, the evolution of reservoir operation policies over time can impact the training data, and such non-stationarity can limit model performance (Lin et al., 2021). This study aims to explore how reasonable knowledge guidance enhances LSTM performance. The loss function of KG-LSTM primarily incorporates general reservoir operation knowledge, which has remained relatively stable during the model construction periods for the three reservoirs, as discussed in Section 3.1.3. Therefore, the significant improvement of KG-LSTM over LSTM provides strong evidence that effective knowledge guidance can help LSTM learn the correct operation rules from evolving data. As shown in Table 4, the improvement of KG-LSTM over LSTM is most pronounced for the XFJR. Being a large, multiyear-regulated reservoir, the XFJR can perform its functions more stably. For example, its large storage capacity enables continuous water retention during the flood season, preventing it from easily surpassing the flood control level, unlike the FSBR and BPZR. This stability ensures that the relevant penalty terms in the loss function remain effective throughout the model training process.

To evaluate the impact of using data from different periods, we trained and tested KG-LSTM model for the XFJR using the data from 1986 to 2006 (maintain a consistent split of 75 % for training and 25 % for testing). The NSE values obtained are 0.68 and 0.66, respectively. These results are comparable to those derived from models trained and tested on data from 1961 to 2006, which yield NSE values of 0.66 and 0.64, respectively. This comparison indicates that the period of data does not significantly affect the model performance. The lower performance of KG-LSTM model for the XFJR compared with FSBR and BPZR is

consistent with the finding of (Chen et al., 2022) who observed that different machine learning models exhibited significantly lower prediction accuracy for multipurpose and multiyear reservoirs with large storage capacities compared to other reservoirs.

The superior accuracy of KG-LSTM can be attributed to two key components: temporal recurrence and process constraints (Fig. 2). LSTM excels in capturing time series patterns and extracting insights from diverse input variables, ensuring robust performance in outflow simulations. Compared to traditional models like LPS and the operation-based scheme proposed by Wu and Chen (2012), LSTM demonstrates clear advantages (Table 4 and Fig. 4) and keep stability when training with different resampled data (Fig. 5). Reservoir operation is a complex process constrained by reservoir functions and operational rules aimed at achieving optimal water resource management.

As the choice of the objective function greatly influences the model performance (Lin et al., 2024), incorporating relevant knowledge-guided constraints into the model's loss function can increase the penalty for unreasonable simulation results, which helps steer the model away from unrealistic predictions and better agree with simulate actual operation behaviors (Zheng et al., 2022). The KG-LSTM model developed in this study supports this statement, as it shows improvements over LSTM in simulating reservoir outflow (see Section 4). Taking the XFJR as an example, KG-LSTM based simulations show a better agreement with flood control requirements, which are part of reservoir operation constraints. The degree of exceedance above the flood control level for KG-LSTM is significantly lower than that of LSTM, with cumulative exceedances of 12.58 m and 14.29 m in model construction period, respectively. KG-LSTM is closer to the observed value of 10.63 m, further emphasizing the impact of flood control constraints. As a soft constraint method, while adding knowledge-guided constraints to the loss function cannot strictly enforce the outflow within specific boundaries, it can increase the penalty for unreasonable simulation results, thereby improving overall performance (Karpatne et al., 2017).

For reservoir-regulated basin streamflow simulation, we propose the hybrid model KG-LSTM-TMPH, which integrates the strengths of deep learning and physics-based models. The model demonstrates significantly improved performance in Longchuan, Heyuan, Lingxia, and Boluo compared to previous studies (Wang et al., 2023). KG-LSTM-TMPH demonstrates best performance at these stations (Fig. 6), particularly during the dry season. Heyuan shows the most significant improvement (Fig. 6f), likely due to its downstream location relative to the XFJR, where KG-LSTM excels. This highlights that incorporating knowledge of reservoir operations enables KG-LSTM-TMPH to more effectively capture the reservoirs' replenishment functions during dry periods.

From the perspective of robustness, KG-LSTM reduce the uncertainty and improve simulation reliability in terms of RW for the XFJR and BPZR (Fig. 5a, b, e, f) compared to standard LSTM. This improvement is attributed to that the XFJR is a multi-year regulated reservoir, while the BPZR is an incomplete multi-year regulated reservoir. Their regulation

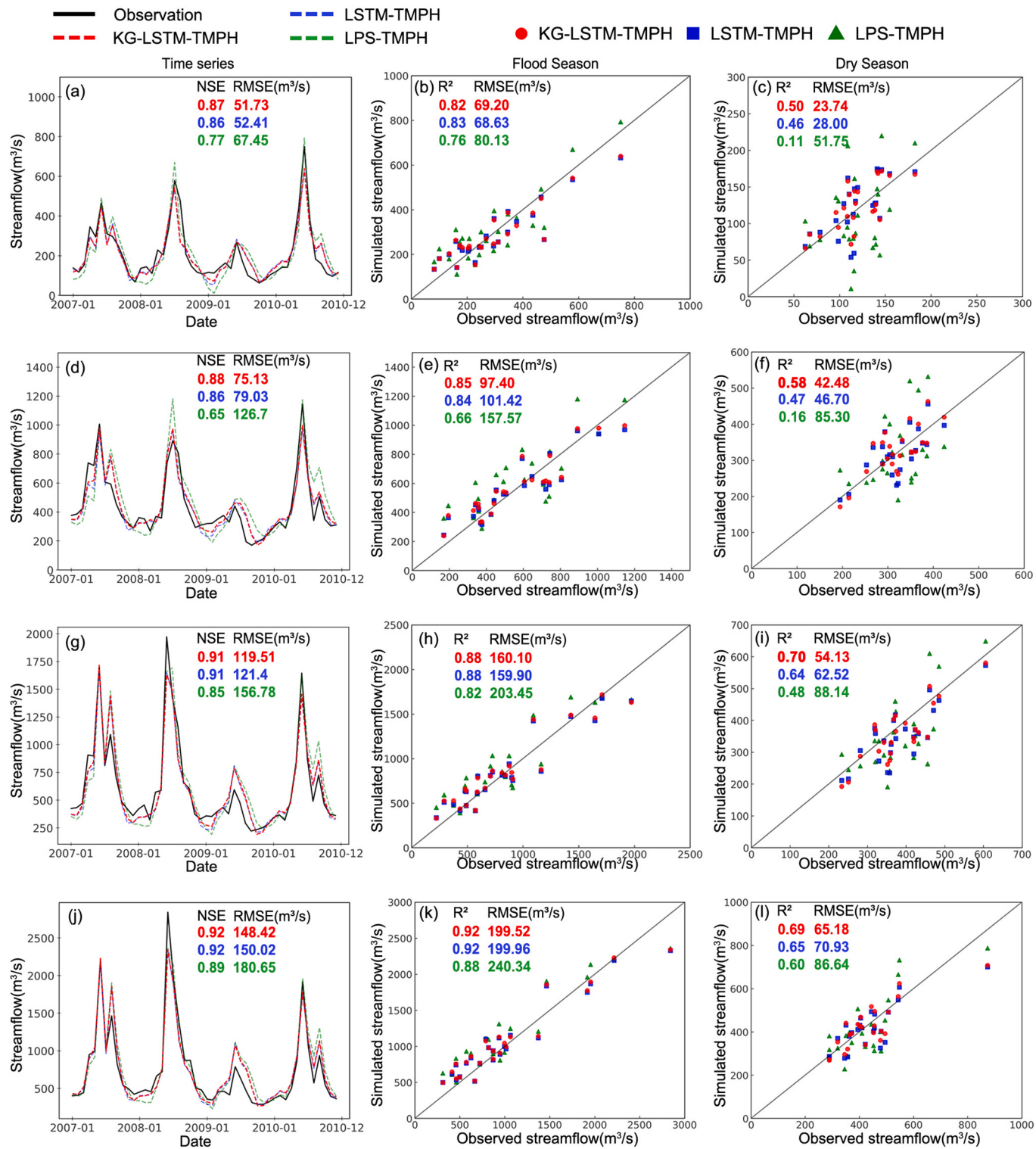


**Fig. 6.** Monthly streamflow time series and scatter plots for flood and dry seasons simulated by the hybrid models at four stations: Longchuan (a, b, c), Heyuan (d, e, f), Lingxia (g, h, i), Boluo (j, k, l), along with corresponding values of NSE, R<sup>2</sup> and RMSE.

strategies enable more reliable water management compared to the FSBR, ensuring that the penalty terms in the loss function align more consistently with actual operational conditions. KG-LSTM's improvement on the FSBR is not evident (Fig. 4c, d and Fig. 5c, d), because the associated penalty term does not effectively operate due to the year-regulated characteristic.

While the reservoir outflow is available through direct measurement,

the simulation of reservoir outflow is still useful, as data may be unavailable due to device malfunctions, and delays in data transmission and processing can arise. In such cases, simulations by data-driven model can provide initial estimates of reservoir outflow since it can replicate expert-driven operation behaviors (Yang et al., 2016), facilitating prompt responses in water resource management. Furthermore, to accurately predict streamflow in reservoir-regulated basins, we need to

estimate future reservoir outflow. By employing the KG-LSTM model proposed in this study, we can enhance the simulation and prediction of reservoir outflow, consequently leading to more accurate streamflow predictions. This capability is crucial for reliable outflow decision-making and effective long-term water resource management in reservoir-regulated basins.

The methodology developed in this study can be applicable to finer time scales, including weekly or daily, which is a focus of our future studies. To achieve this, different input variables and associated time lags for the reservoir outflow need to be reconsidered, as the influencing

factors and the corresponding lead times at weekly or daily scales differ from those at the monthly scale. For instance, the hydrological year is no longer a valid input variable for daily reservoir operations. Additionally, refining the operation rules to create a more rational loss function will help ensure that short-term operational information and characteristics are adequately captured. The hydrological model must also run at the finer temporal scale to provide short-term inflow predictions. In this context, a routing model should be integrated in the hydrological model to accurately predict the inflow and its timing.

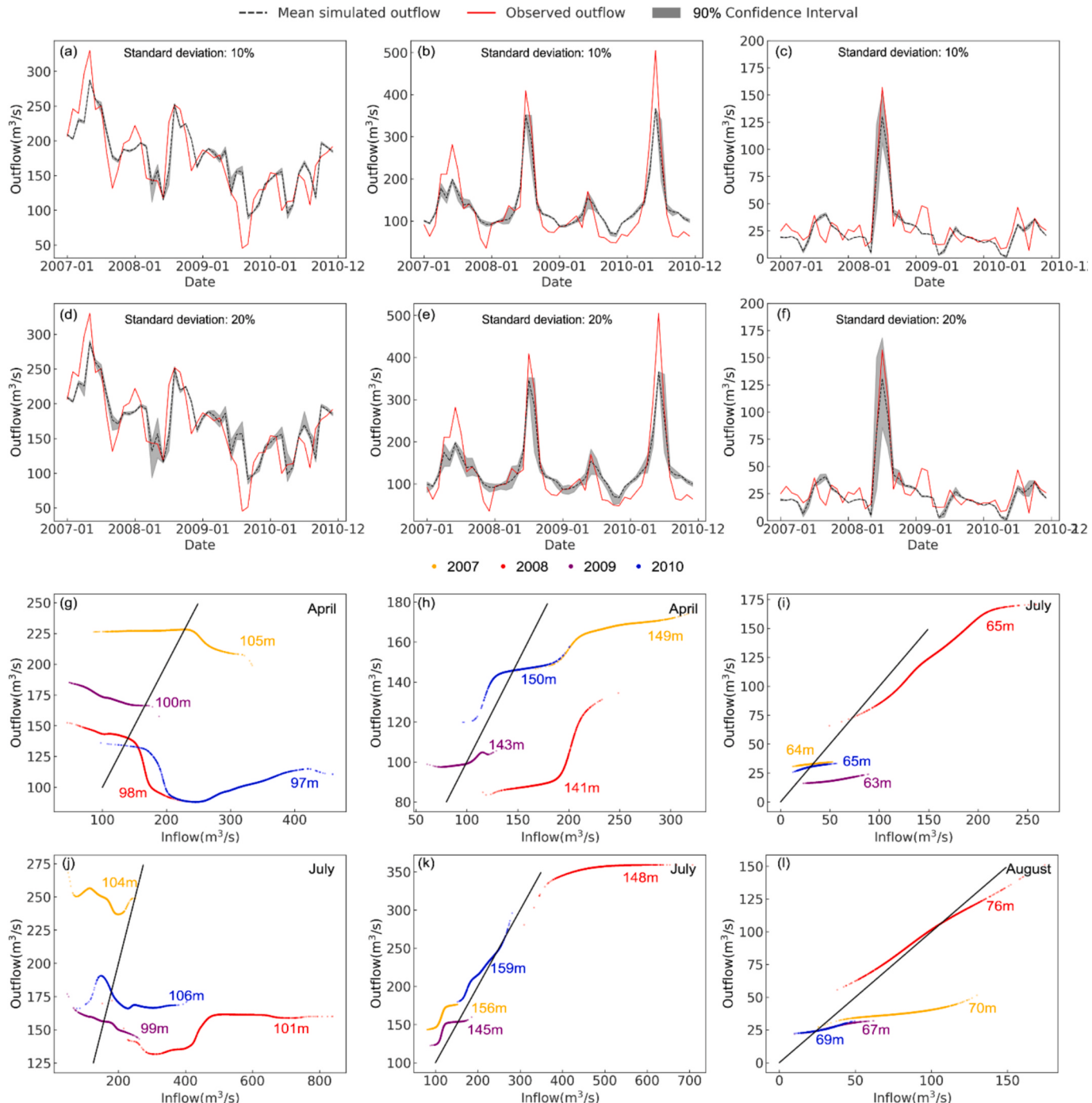


**Fig. 7.** Monthly reservoir outflow time series simulated by KG-LSTM, with impact by inflow simulation error with standard deviations of 10% and 20% for three reservoirs: XFJR (a, d), FSBR (b, e), BPZR (c, f). The grey shading represents the 90% uncertainty intervals. The relationship between inflow and outflow are presented for April (g) and July (j) at XFJR, for April (h) and July (k) at FSBR, and for July (i) and August (l) at BPZR. The numbers in panels g-l represent the initial reservoir water levels for each respective month. The black lines represent the equality line, where inflow equals outflow.

## 5.2. The propagation of inflow errors to outflow simulations through KG-LSTM

The simulation of inflow to reservoirs often encounters error in reality due to challenges in accurately predicting meteorological conditions. To investigate how these errors propagate to the simulation of reservoir outflow through the KG-KSTM model, we assume these errors are random and can be modeled with a normal distribution with a mean of 0 and a standard deviation derived from the observed inflow data (Baker, 1977). Monte Carlo method is used to generate inflow samples from the distribution, using a sample size of 2000 and the simulating errors with standard deviations of 10 % and 20 % as indicated in the previous study (Yang et al., 2019). Fig. 7a-f show the time series of reservoir outflow simulated by KG-LSTM with inflow simulation errors. Generally, the uncertainties of the simulated reservoir outflow increase as the error of inflow simulation increases. However, the impact of inflow error varies with reservoirs in different month. To better understand how the inflow errors propagation to outflow simulations in those highly-impacted months, we present the relationship between simulated outflow and inflow in Fig. 7g-l.

For the XFJR (Fig. 7a, d), inflow errors have the most pronounced impact on reservoir outflow during April and May, coinciding with the onset of the flood season. After replenishing water in the dry season, reservoirs with smaller storage capacity (i.e., FSBR and BPZR) are in low water levels. Thus, larger XFJR plays a more crucial role in replenishment during dry periods, with its outflow being significantly affected by inflow errors. The inflow-outflow relationship in April shown in Fig. 7g explains how the inflow errors propagation to outflow simulations (since the relationship very similar for April and May, we focus April only). In 2007, the water level (105 m) was high enough for KG-LSTM to maintain a consistently high outflow for replenishment, regardless of inflow magnitude, resulting minimal impact from inflow errors. In contrast, in other years, when initial water levels were below 100 m, outflow simulations remained stable under when inflows were underestimated, but decreased sharply with overestimated inflows, eventually stabilizing at a low outflow. This is because KG-LSTM tends to impound water when the basin's water is sufficient and its own water level is low. In July (Fig. 7j), outflow simulations are affected by inflow errors, as flood risk management becomes the primary concern. When water levels are high, outflows are regulated to remain below the flood limit, resulting in stable high outflows regardless of inflow errors. Conversely, when water levels are low, the XFJR tends to focus on impoundment due to its larger capacity, causing KG-LSTM to reduce outflow when inflow are overestimated.

For the FSBR, inflow errors significantly impact outflow across all periods, particularly in the flood season in April, May, July, and August. Flood control is the primary function of the FSBR, and its small capacity magnifies the impact of inflow errors on outflow simulations. The inflow-outflow relationships for April and July, shown in Fig. 7h and 7k, illustrate this impact (since the relationships for April/May and July/August are similar, we focus on April and July.). Outflow simulations for the FSBR generally increase with overestimated inflows at any water level, which contrasts with the behavior of the XFJR. This is because the FSBR needs to increase outflows in response to overestimated inflows to balance flood control and impoundment functions. Additionally, the FSBR is more significantly affected by inflow errors during the dry season due to its annual regulation capacity, which lacks the ability to maintain a relatively stable outflow compared to the XFJR (the multi-year regulated reservoir) and BPZR (the incompletely multiyear regulated reservoir).

For the BPZR, the impact of inflow errors is particularly significant in July (Fig. 7i) and August (Fig. 7l). In these months, when inflows are overestimated, the simulated outflow increases and eventually stabilizes at a constant value, resembling the pattern in observed the FSBR. However, the rate of change in the BPZR is slightly lower than that in the FSBR, due to its incomplete multi-year regulation capacity, which allows

it to impound more water compared to the FSBR. The BPZR is highly influenced by inflow errors in August due to its proximity to the coastline, making it particularly susceptible to typhoons. A typical example occurred in August 2008 when typhoons impacted the coastline of Guangdong Province, causing the water level to rise to 76 m, the flood limit level. As a result, the outflow became more sensitive to inflow errors, with the rate of change in outflow increasing significantly, approaching the inflow rate to prevent further rise in the water level.

## 6. Conclusion

This study proposes an LSTM model guided by reservoir operation knowledge (KG-LSTM) to simulate reservoir outflows, using the Dongjiang River Basin in China as a case study. The KG-LSTM framework consists of two components: an optimized standard LSTM and a loss function that considers reservoir operation knowledge, while the traditional reservoir model LPS is used as benchmark for KG-LSTM. The bootstrap method is then employed for KG-LSTM's model uncertainty analysis. A hybrid approach combining KG-LSTM with the TMPH hydrological model (KG-LSTM-TMPH) is proposed for streamflow simulation in reservoir-regulated basins. The propagation of inflow errors to outflow simulations through KG-LSTM is also studied. The results show that:

- 1) LSTM-based models outperform LPS in the three reservoirs and KG-LSTM can better capture reservoir outflow dynamics compared to the standard LSTM model, particularly in the multi-year regulated XFJR, where it improves Nash-Sutcliffe efficiency (NSE) from 0.59 to 0.64, reduces root mean squared error (RMSE) from 55.59 m<sup>3</sup>/s to 54.84 m<sup>3</sup>/s during the testing period. KG-LSTM has less model uncertainty, decreasing the relative width (RW) from 0.55 to 0.51 in the XFJR, from 0.48 to 0.44 in the BPZR, while with limited change in the FSBR. KG-LSTM's improvement on the FSBR is limited, as it is a yearly regulated reservoir that allocates water storage during the flood season for the dry season, resulting in less stable functionality and frequent unreasonable penalties.
- 2) For streamflow simulation, KG-LSTM-TMPH performs best across all four stations, achieving NSE values of approximately 0.87, 0.88, 0.91, and 0.92 at Longchuan, Heyuan, Lingxia, and Boluo stations, respectively. In dry season, KG-LSTM-TMPH demonstrates substantial improvement over LSTM-TMPH, increasing R<sup>2</sup> by + 0.11 and reducing RMSE with -4.22 m<sup>3</sup>/s at Heyuan station. For simulation in dry season, KG-LSTM-TMPH can efficiently reduce the underestimation in outflow compared to LSTM-TMPH in all stations.
- 3) The impact of inflow errors on simulated outflow varies across reservoirs. Inflow errors impact outflow most significantly for the XFJR in April and May, for the FSBR throughout the year (especially in April, May, July, and August), and for the BPZR primarily in July and August. As the overestimation of inflow errors increases, the XFJR tends to decrease outflow, the FSBR increases outflow rapidly, while the BPZR exhibits a more pronounced rate of change under high inflow conditions.

By integrating historical data on reservoir functions and operation rules, this study effectively embeds reservoir operation knowledge into the LSTM model, forming KG-LSTM reservoir outflow model. When combined with weather forecasts, this model promises more reliable hydrological predictions, which would be beneficial for flood prevention and water resource management in the basin. The principles used in developing this model could also serve as a valuable reference for constructing similar models in other reservoir-regulated basins.

## CRediT authorship contribution statement

**Runting Chen:** Writing – original draft, Methodology, Formal analysis, Data curation, Conceptualization. **Dagang Wang:** Writing –

original draft, Project administration, Methodology, Conceptualization. **Yiwen Mei**: Writing – review & editing. **Yongen Lin**: Resources, Data curation. **Zequn Lin**: Writing – review & editing. **Zhi Zhang**: Writing – review & editing, Conceptualization. **Shengjie Zhuang**: Data curation. **Jinxin Zhu**: Writing – review & editing. **Jonghun Kam**: Writing – review & editing. **Yiping Wu**: Writing – review & editing. **Guoping Tang**: Writing – review & editing.

## Declaration of competing interest

The authors declare that they have no known competing financial interests or personal relationships that could have appeared to influence the work reported in this paper.

## Acknowledgments

This work is supported by the National Natural Science Foundation of China (42301021, 52079151, and 52111540261) and the National Key R&D Program of China (2024YFC3013302).

## Data availability

Data will be made available on request.

## References

- Allawi, M.F., Jaafar, O., Hamzah, F.M., Abdullah, S.M.S., El-shafie, A., 2018. Review on applications of artificial intelligence methods for dam and reservoir-hydro-environment models. *Environmental Science and Pollution Research* 25 (14), 13446–13469.
- Anand, J., Gosain, A., Khosa, R., 2018. Optimisation of multipurpose reservoir operation by coupling soil and water assessment tool (SWAT) and genetic algorithm for optimal operating policy (case study: Ganga River Basin). *Sustainability* 10 (5).
- Baker, K.R., 1977. An Experimental Study of the Effectiveness of Rolling Schedules in Production Planning 8 (1), 19–27.
- Bock, A.R., Farmer, W.H., Hay, L.E., 2018. Quantifying uncertainty in simulated streamflow and runoff from a continental-scale monthly water balance model. *Advances in Water Resources* 122, 166–175. <https://doi.org/10.1016/j.advwatres.2018.10.005>.
- Chang, F.-J., Guo, S., 2020. Advances in hydrologic forecasts and water resources management. *Water* 12 (6).
- Chen, Y., Li, D., Zhao, Q., Cai, X., 2022. Developing a generic data-driven reservoir operation model. *Advances in Water Resources* 167.
- García-Feal, O., González-Cao, J., Fernández-Nóvoa, D., Astray Dopazo, G., Gómez-Gesteira, M., 2022. Comparison of machine learning techniques for reservoir outflow forecasting. *Natural Hazards and Earth System Sciences* 22 (12), 3859–3874.
- Goodell, C.R., Wahlin, B., 2009. Dynamic and level pool reservoir drawdown: A practical comparison for dam breach modeling. In: Proc., 33rd IAHR Congress, Water Engineering for a Sustainable Environment, pp. 6843–6850.
- Gopala, S.P., Kawamura, A., Amaguchi, H., Takasaki, T., Azhikodan, G., 2019. A bootstrap approach for the parameter uncertainty of an urban-specific rainfall-runoff model. *Journal of Hydrology* 579.
- Haddeland, I., Skjaug, T., Lettenmaier, D.P., 2006. Anthropogenic impacts on continental surface water fluxes. *Geophysical Research Letters* 33 (8).
- Hanasaki, N., Kanae, S., Oki, T., 2006. A reservoir operation scheme for global river routing models. *Journal of Hydrology* 327 (1–2), 22–41.
- Hochreiter, S., Schmidhuber, J., 1997. Long short-term memory. *Neural Comput.* 9 (8), 1735–1780.
- Karpatne, A., Attluri, G., Faghnoos, J.H., Steinbach, M., Banerjee, A., Ganguly, A., Shekhar, S., Samatova, N., Kumar, V., 2017. Theory-guided data science: a new paradigm for scientific discovery from data. *IEEE Trans. Knowl. Data Eng.* 29 (10), 2318–2331.
- Kumar, S., Tiwari, M.K., Chatterjee, C., Mishra, A., 2015. Reservoir inflow forecasting using ensemble models based on neural networks, wavelet analysis and bootstrap method. *Water Resources Management* 29 (13), 4863–4883.
- Lin, Y.E., Wang, D.G., Wang, G.L., Qiu, J.X., Long, K.H., Du, Y., Xie, H.H., Wei, Z.W., Shangguan, W., Dai, Y.J., 2021. A hybrid deep learning algorithm and its application to streamflow prediction. *Journal of Hydrology* 601.
- Lin, Y.E., Wang, D.G., Zhu, J.X., Sun, W., Shen, C.P., Wei, S.G., 2024. Development of objective function-based ensemble model for streamflow forecasts. *Journal of Hydrology* 632.
- Liu, Y., Li, J., Li, H., Yang, B., Liu, W., 2019. Effect of the Three Gorges reservoir operation on flood inter-jacking in the confluence section of rivers and lakes. *Journal of Water Resources and Water Engineering* 30 (2), 114.
- Ma, L., Liu, Y., Zhang, X., Ye, Y., Yin, G., Johnson, B.A., 2019. Deep learning in remote sensing applications: A meta-analysis and review. *Ispis Journal of Photogrammetry and Remote Sensing* 152, 166–177.
- Nash, J.E., Sutcliffe, J.V., 1970. River flow forecasting through conceptual models part I—a discussion of principles. *Journal of Hydrology* 10 (3), 282–290. [https://doi.org/10.1016/0022-1694\(70\)90255-6](https://doi.org/10.1016/0022-1694(70)90255-6).
- Nohara, D., Hori, T., 2018. Reservoir operation for water supply considering operational ensemble hydrological predictions. *Journal of Disaster Research* 13 (4), 650–659.
- Ozdogan-Sarikoc, G., Sarikoc, M., Celik, M., Dadaser-Celik, F., 2023. Reservoir volume forecasting using artificial intelligence-based models: artificial neural networks, support vector regression, and long short-term memory. *Journal of Hydrology* 616.
- Peng, S., Jiang, H., Wang, H., Alwaged, H., Zhou, Y., Sebdani, M.M., Yao, Y.-D., 2019. Modulation classification based on signal constellation diagrams and deep learning. *Ieee Transactions on Neural Networks and Learning Systems* 30 (3), 718–727.
- Qie, G., Zhang, Z., Getahun, E., Mamer, E.A., 2023. Comparison of machine learning models performance on simulating reservoir outflow: a case study of two reservoirs in Illinois, USA. *Journal of the American Water Resources Association* 59 (3), 554–570.
- Shen, C.P., Laloy, E., Elshorbagy, A., Albert, A., Bales, J., Chang, F.J., Ganguly, S., Hsu, K. L., Kifer, D., Fang, Z., Fang, K., Li, D.F., Li, X.D., Tsai, W.P., 2018. HESS Opinions: Incubating deep-learning-powered hydrologic science advances as a community. *Hydrology and Earth System Sciences* 22 (11), 5639–5656.
- Soria-Lopez, A., Sobrido-Pouso, C., Mejuto, J.C., Astray, G., 2023. Assessment of different machine learning methods for reservoir outflow forecasting. *Water* 15 (19).
- Sushanth, K., Mishra, A., Mukhopadhyay, P., Singh, R., 2023. Real-time streamflow forecasting in a reservoir-regulated river basin using explainable machine learning and conceptual reservoir module. *Sci Total Environ* 861, 160680.
- Turner, S.W.D., Steyaert, J.C., Condon, L., Voisin, N., 2021. Water storage and release policies for all large reservoirs of conterminous United States. *Journal of Hydrology* 603.
- Wang, K., Shi, H., Chen, J., Li, T., 2019. An improved operation-based reservoir scheme integrated with variable infiltration capacity model for multiyear and multipurpose reservoirs. *Journal of Hydrology* 571, 365–375.
- Wang, Z., He, Y., Li, W., Chen, X., Yang, P., Bai, X., 2023. A generalized reservoir module for SWAT applications in watersheds regulated by reservoirs. *Journal of Hydrology* 616.
- Wang, Z., Si, Y., Chu, H., 2022. Daily Streamflow prediction and uncertainty using a long short-term memory (LSTM) network coupled with bootstrap. *Water Resources Management* 36 (12), 4575–4590.
- Wu, Y., Chen, J., 2012. An operation-based scheme for a multiyear and multipurpose reservoir to enhance macroscale hydrologic models. *Journal of Hydrometeorology* 13 (1), 270–283.
- Xie, T., Zhang, G., Hou, J.W., Xie, J.C., Lv, M., Liu, F.C., 2019. Hybrid forecasting model for non-stationary daily runoff series: A case study in the Han River Basin, China. *Journal of Hydrology* 577, 15.
- Xu, W.F., Liu, P., Cheng, L., Zhou, Y., Xia, Q., Gong, Y., Liu, Y.N., 2021. Multi-step wind speed prediction by combining a WRF simulation and an error correction strategy. *Renew. Energy* 163, 772–782.
- Xu, Y.H., Hu, C.H., Wu, Q., Jian, S.Q., Li, Z.C., Chen, Y.Q., Zhang, G.D., Zhang, Z.X., Wang, S.L., 2022. Research on particle swarm optimization in LSTM neural networks for rainfall-runoff simulation. *Journal of Hydrology* 608, 11.
- Yang, S., Yang, D., Chen, J., Zhao, B., 2019. Real-time reservoir operation using recurrent neural networks and inflow forecast from a distributed hydrological model. *Journal of Hydrology* 579.
- Yang, T., Gao, X., Sorooshian, S., Li, X., 2016. Simulating California Reservoir Operation Using the Classification and Regression-tree Algorithm Combined with a Shuffled Cross-validation Scheme 52 (3), 1626–1651.
- Zhang, D., Lin, J., Peng, Q., Wang, D., Yang, T., Sorooshian, S., Liu, X., Zhuang, J., 2018. Modeling and simulating of reservoir operation using the artificial neural network, support vector regression, deep learning algorithm. *Journal of Hydrology* 565, 720–736.
- Zhang, Z., Lu, W., Chu, H., Cheng, W., Zhao, Y., 2014. Uncertainty analysis of hydrological model parameters based on the bootstrap method: A case study of the SWAT model applied to the Dongliao River Watershed, Jilin Province, Northeastern China. *Science China-Technological Sciences* 57 (1), 219–229.
- Zhao, G., Gao, H., Naz, B.S., Kao, S.-C., Voisin, N., 2016. Integrating a reservoir regulation scheme into a spatially distributed hydrological model. *Advances in Water Resources* 98, 16–31.
- Zheng, Y.L., Liu, P., Cheng, L., Xie, K., Lou, W., Li, X., Luo, X.R., Cheng, Q., Han, D.Y., Zhang, W., 2022. Extracting operation behaviors of cascade reservoirs using physics-guided long-short term memory networks. *Journal of Hydrology-Regional Studies* 40.
- Zou, Y., Yan, B., Feng, B., Zhang, J., Tang, Y., 2023. A three-parameter hydrological model for monthly runoff simulation—a case study of upper Hanjiang River Basin. *Water* 15 (3).